

Gene Expression Analysis of Zebrafish Melanocytes, Iridophores, and Retinal Pigmented Epithelium Reveals Indicators of Biological Function and Developmental Origin

Charles W. Higdon*, Robi D. Mitra, Stephen L. Johnson*

Department of Genetics, Washington University, St. Louis, Missouri, United States of America

Abstract

In order to facilitate understanding of pigment cell biology, we developed a method to concomitantly purify melanocytes, iridophores, and retinal pigmented epithelium from zebrafish, and analyzed their transcriptomes. Comparing expression data from these cell types and whole embryos allowed us to reveal gene expression co-enrichment in melanocytes and retinal pigmented epithelium, as well as in melanocytes and iridophores. We found 214 genes co-enriched in melanocytes and retinal pigmented epithelium, indicating the shared functions of melanin-producing cells. We found 62 genes significantly co-enriched in melanocytes and iridophores, illustrative of their shared developmental origins from the neural crest. This is also the first analysis of the iridophore transcriptome. Gene expression analysis for iridophores revealed extensive enrichment of specific enzymes to coordinate production of their guanine-based reflective pigment. We speculate the coordinated upregulation of specific enzymes from several metabolic pathways recycles the rate-limiting substrate for purine synthesis, phosphoribosyl pyrophosphate, thus constituting a guanine cycle. The purification procedure and expression analysis described here, along with the accompanying transcriptome-wide expression data, provide the first mRNA sequencing data for multiple purified zebrafish pigment cell types, and will be a useful resource for further studies of pigment cell biology.

Citation: Higdon CW, Mitra RD, Johnson SL (2013) Gene Expression Analysis of Zebrafish Melanocytes, Iridophores, and Retinal Pigmented Epithelium Reveals Indicators of Biological Function and Developmental Origin. PLoS ONE 8(7): e67801. doi:10.1371/journal.pone.0067801

Editor: Yuk Fai Leung, Purdue University, United States of America

Received: February 4, 2013; **Accepted:** May 23, 2013; **Published:** July 9, 2013

Copyright: © 2013 Higdon et al. This is an open-access article distributed under the terms of the Creative Commons Attribution License, which permits unrestricted use, distribution, and reproduction in any medium, provided the original author and source are credited.

Funding: This work was made possible by grants from the National Institutes of Health (NIH) (RO1-GM56988) the W.M. Keck Foundation (<http://www.wmkeck.org>). The funders had no role in study design, data collection and analysis, decision to publish, or preparation of the manuscript.

Competing Interests: The authors have declared that no competing interests exist.

* E-mail: cwhigdon@wustl.edu (CWH); sjohnson@genetics.wustl.edu (SLJ)

Introduction

Pigment cells serve as useful models for understanding many aspects of developmental and cell biology. For example, melanocytes are pigment cells studied to understand cell specification, migration, differentiation, survival, regeneration, organelle transport, secretion, and disease [1–15]. Melanocytes produce melanin, which in humans serves as a UV protectant in skin [16]. Melanocytes also have roles in other organs such as the ear, brain, heart, and adipose tissue [17,18]. The incidence of melanomas, a disease of melanocytes and the most lethal form of skin cancer, is also increasing [19]. Methods to isolate and culture melanocytes for *in vitro* studies have been informative for understanding melanocyte biology [20,21]. *In vivo* studies of melanocyte biology and melanoma dynamics have been aided by the identification of mutants in mice and zebrafish [22–25]. Given the utility of zebrafish melanocytes to understand cell biology and disease, the transcriptome-wide characterization of genes expressed in zebrafish pigment cells would be a significant resource.

In mammalian systems, melanocytes are the only neural crest-derived pigment cell type found in the dermis. In contrast, several neural crest-derived pigment cells are found in zebrafish and other poikilotherms, including reflective iridophores [5]. Several re-

quirements for iridophore development from the neural crest are known [5,26,27]. However, it is unknown if markers of neural crest identity persist in iridophores following development, and whether these markers are shared by other neural crest-derived pigment cells, such as melanocytes. A further question in iridophore biology is how the guanine-based pigment is produced [28,29]. Zebrafish bearing mutations in the *de novo* purine synthesis enzymes *gart* and *paics* have iridophore defects, indicating purine synthesis is important for iridophore pigmentation [30]. Identifying a possible mechanism by which iridophores produce an abundance of guanine for pigment formation while maintaining adequate supplies of purines for DNA and RNA production will be informative for cell biology.

Another pigment cell type shared by mammalian and poikilothermic vertebrates is the retinal pigmented epithelium (RPE). The RPE is a group of melanin-producing cells found in the vertebrate eye. The RPE develops from the eye primordium, and is continuous with the layer of cells that forms the iris [31]. The RPE is critical for eye development and retinal health. It provides trophic support and recycles wastes from the photoreceptors of the retina [32]. The RPE forms part of the blood-retina barrier, providing the eye with an immune-privileged status [33]. Defects in the RPE contribute to diseases such as macular degeneration

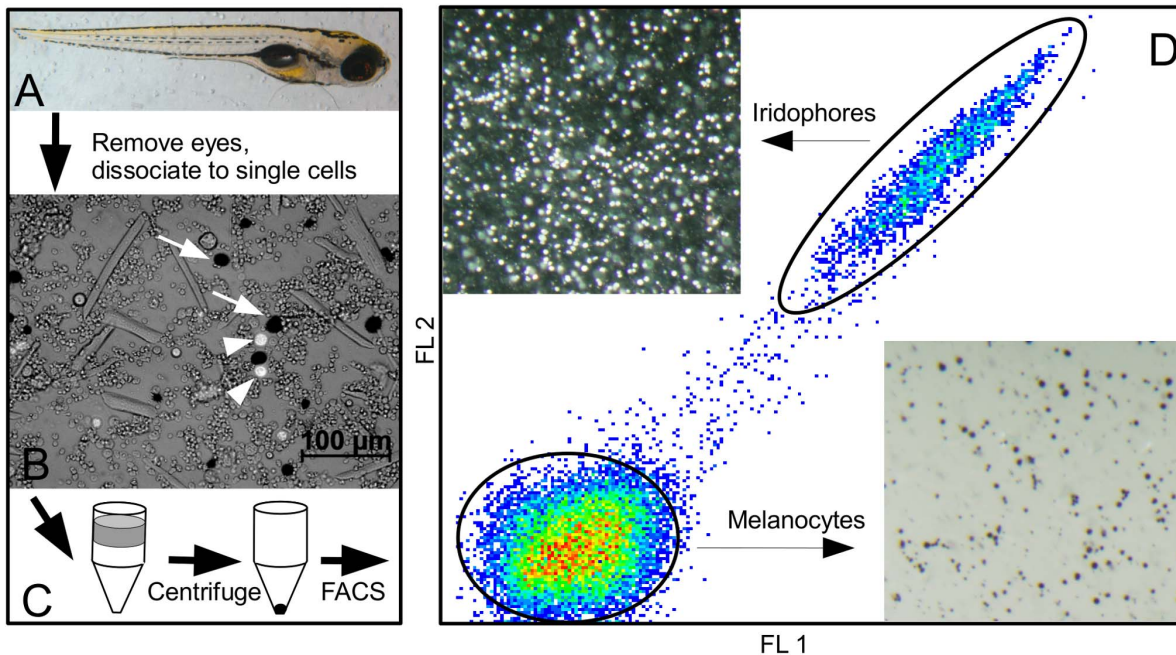


Figure 1. Purification procedure for melanocytes, iridophores, and retinal pigmented epithelium. Zebrafish are grown to the desired time point; shown in (A) is a six day old fish. (B) Fish are dissociated to a single cell suspension; black melanocytes (arrows) and reflective iridophores (arrowheads) are visible as a small percentage of all cells. (C) Cells are placed atop a Percoll density gradient and centrifuged. (D) The resulting cell pellet is resuspended and analyzed by FACS. Shown is a characteristic FACS plot demonstrating the relative positions of melanocyte and iridophore gates (ovals). Sorted iridophores are shown on the upper left of (D) under incident light. Sorted melanocytes are on the lower right using trans-illumination.

doi:10.1371/journal.pone.0067801.g001

and retinitis pigmentosa, which result in vision problems [34,35]. Previous descriptions of gene expression in the RPE of zebrafish, chicken, and human have elucidated many of the genes playing roles in RPE biology [36–38]. Many of these genes are responsible for producing melanin, and defects in melanin production are often associated with reduced visual function [39]. However, it is unknown whether RPE and melanocytes use different pathways of melanin production, or if they are essentially identical. This information would be useful for understanding RPE biology, and would also inform future examinations of regulatory control for genes expressed in one or both cell types.

In order to facilitate understanding of these pigment cells, we developed a robust method to isolate these three pigment cell types from zebrafish embryos, followed by mRNA sequencing and transcriptome analysis. This purification procedure relies on the inherent densities of melanin and guanine-filled cells; hence it can be used without other complicated lineage markers. Here, we report the co-enrichment and cell-type specific gene expression profiles of melanocytes, iridophores, and RPE from embryonic zebrafish. While RPE and iridophores do not exhibit significant overlap of enriched gene expression, our analysis reveals considerable overlap among pairs of pigment cell types indicative of their common origin or function. Genes enriched in both the melanocyte and RPE lineages contain genes in the melanin-production pathway, and suggest a more complete picture of melanin-producing machinery is contained within this set. Similarly, expression co-enrichment in melanocytes and iridophores are reflective of their neural crest origin, and suggest genes in this set may be specific to neural crest identity. Furthermore, this is the first characterization of the iridophore transcriptome. We found that iridophores specifically upregulate the guanine portion of *de novo* purine synthesis, as well as specific enzymes from

other metabolic pathways that aid in producing the iridophore guanine-based reflective pigment. In addition to the analysis presented here, this procedure and accompanying data provide a significant resource for further biological discovery in pigment cells.

Materials and Methods

Zebrafish Strain and Sample Collection Time Points

This study was carried out in accordance with the Washington University Animal Use Committee guidelines under approved protocol #20110236. Zebrafish were reared and bred according to standard protocols [40]. The fish used in this study were homozygous for a temperature sensitive allele of microphthalmia transcription factor (*mitfa*^{ts7}) [41]. This mutant facilitated the collection of RPE, as *mitfa* is not required for RPE development in zebrafish [41]. Melanocytes, iridophores, and RPE develop normally at 25°C in *mitfa*^{ts7}. When held at 32°C, the neural crest-derived melanocytes do not develop, but RPE and iridophores develop normally. All melanocyte and iridophore samples were incubated at 25°C prior to collection. We note the possibility that *mitfa* may be partially compromised by aberrant splicing products in this mutant at permissive temperatures, but following development at 25°C, melanocyte numbers, morphology, and pigmentation are indistinguishable from wild-type zebrafish [41]. Embryos used for RPE samples were incubated at either 25°C or 32°C until the equivalent of 3–5 days at 28.5°C, as indicated in Table S1 [42]. It should be noted that at stages later than 5dpf, choroidal melanocytes may be present adjacent to the RPE. Only one of the five RPE cDNA libraries was prepared later than 5dpf, as indicated in Table S1. We did not have separate markers to identify contamination from eye-associated neural

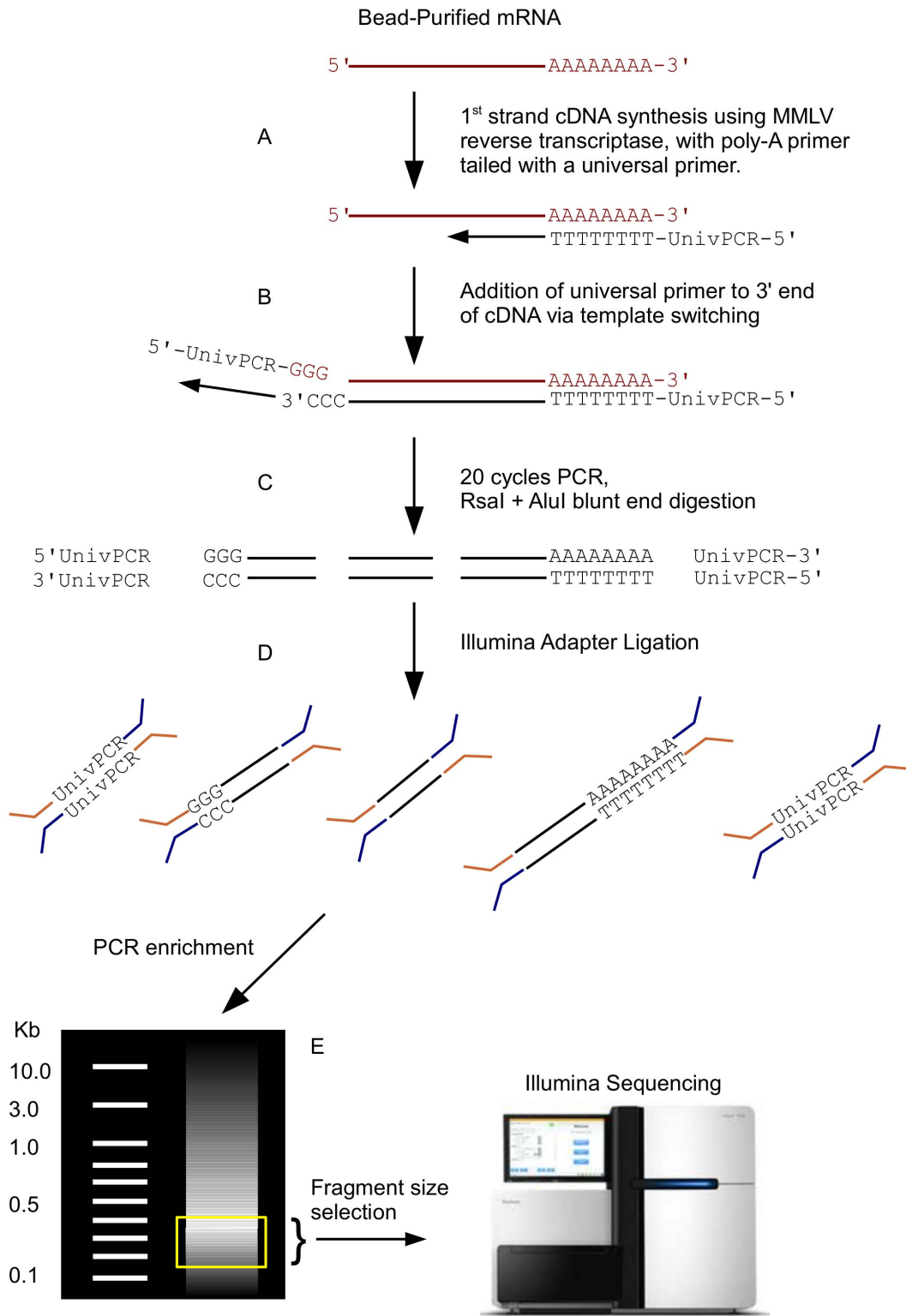


Figure 2. Schematic of cDNA library preparation. PolyA-selected mRNA (in red) is reverse transcribed using a polyT primer tailed with a universal primer (A). See Table S3 for primer sequences. MMLV reverse transcriptase adds cytosines to the 3' end of the 1st strand cDNA (in black), allowing for template switching and addition of the 3' universal primer (B). PCR amplification of the library is followed by RsaI and AluI enzymatic digestion of cDNAs (C), followed by the standard Illumina library preparation steps of end-repair, a single adenine addition, Y-adapter ligation (D), PCR enrichment, and size selection (mock gel shown in E with yellow box indicating area of gel removed for DNA extraction), prior to flowcell generation and sequencing.

doi:10.1371/journal.pone.0067801.g002

crest-derived melanocytes, or choroidal melanocytes in our RPE preparations. If present, we expect the contribution to total gene expression in the RPE samples to exhibit high variance, and found to be insignificant by Student's T-test upon comparison to the other cell types. However, we find the later stage RPE library to be highly correlated overall with the earlier stages, indicating that extensive contamination from choroidal melanocytes is unlikely ($r = 0.92$, Figure S1a). It was a further possibility that many large changes in gene expression would be present in RPE samples held at restrictive and permissive temperatures for *mifa*. We found that samples held at the low and high temperatures exhibited a high degree of similarity ($r = 0.89$), indicating that most genes are not significantly different at the two temperatures (Figure S1b). We also expect some genes to change during development between 3 and 5 days post fertilization. Upon inspection of melanocyte samples prepared at several time points, we find correlations increase with increasing developmental age of the embryos (Figure S2). We do not have the statistical power to confidently track developmental changes in gene expression within specific cell types, but we make the data available for all individual libraries to facilitate further investigation (Table S2).

Cell Dissociation and Pigment Cell Enrichment

Figure 1 depicts the general procedure for pigment cell purification. Fish were anesthetized with Tricaine, rinsed with Ca-, Mg- DPBS (Sigma, D8537), and immersed in 100 mL TrypLE Express (Invitrogen, 12604039) per 1000 fish. Fish were incubated at 37°C and shaken at 100rpm for 15–20 minutes, followed by trituration with a Pasteur pipette to remove eyes from larva. After separation of eyes and larva, each group was placed in

TrypLE Express and shaken at 100rpm at 37°C for 1–1.5 hr. Dissociated cells were filtered through a 120 μ M screen into 50 mL tubes. Remaining intact tissue was triturated 10–20 times, and again filtered through a 120 μ M screen into the dissociated cells. Dissociated cells were pelleted in a swinging bucket rotor (Eppendorf 5810 R) at 500 relative centrifugal force (rcf) for 5 minutes at 4°C, then resuspended in 1 mL cold isotonic Percoll (Sigma, P1644) by gentle pipetting. Isotonic Percoll was prepared by mixing 1 part 10X PBS with 9 parts Percoll. Resuspended cells were transferred to 1.6 mL Eppendorf tubes and spun at 2000rcf for 5 minutes at 4°C in a swinging bucket rotor for isopycnic separation. Pigment cells in the pellet were then resuspended in 400 μ L of ice cold DPBS with 2% fetal calf serum (FCS), and placed onto preformed Percoll density gradients. Preformed gradients were prepared via centrifugation of 1 mL aliquots of isotonic Percoll in 1.6 mL tubes at 10,000rcf for 15 minutes at 4°C in a fixed angle micro-centrifuge (Eppendorf 5415 R). Tubes containing preformed Percoll gradients with overlying cell suspensions were centrifuged in a swinging bucket rotor at 2000rcf for 10 minutes at 4°C. Following centrifugation, overlying Percoll was aspirated, leaving the final 100 μ L containing the pigment cell pellet. Cells were resuspended with 50 μ L of cold DPBS with 2% FCS and transferred to a clean 1.6 mL tube containing 500 μ L of cold DPBS with 2% FCS, and kept on ice until mRNA extraction or FACS.

FACS

We used the inherent properties of the pigmented cells to perform Fluorescence-Activated Cell Sorting (FACS). Following resuspension in 500 μ L cold DPBS with 2% FCS, the enriched

Table 1. Candidate control genes are differentially expressed.

	RPKM Counts			Student's T-test p-Values		
	Melanocyte	RPE	Iridophore	Melanocyte vs. RPE	Melanocyte vs. Iridophore	RPE vs. Iridophore
Melanocyte Genes						
<i>gch2</i>	54.25	9.81	1.58	0.007	0.002	0.113
<i>mlphb</i>	187.84	7.96	1.39	0.004	0.003	0.251
<i>kita</i>	3.78	0.39	0.02	0.019	0.011	0.076
Melanin Synthesis						
<i>pmela</i>	15177.25	4244.20	148.90	0.051	0.011	0.031
<i>dct</i>	14134.12	6406.98	402.47	0.025	0.000	0.028
<i>tyrp1b</i>	12354.09	3769.95	200.99	0.026	0.004	0.009
Iridophore Genes						
<i>atic</i>	7.60	9.63	467.16	0.664	0.010	0.010
<i>ednrb1</i>	4.44	1.72	28.63	0.110	0.018	0.013
<i>ltk</i>	0.02	0.20	4.02	0.138	0.002	0.002
Neural Crest						
<i>sox10</i>	7.57	1.76	13.00	0.010	0.078	0.005
<i>foxd3</i>	3.03	0.35	6.41	0.012	0.237	0.063
<i>snai2</i>	4.26	0.79	4.08	0.016	0.904	0.020
RPE Genes						
<i>pax6a</i>	10.04	47.48	0.73	0.098	0.004	0.055
<i>nr2e1</i>	0.75	2.41	0.05	0.189	0.041	0.086
<i>myo7ab</i>	1.89	3.32	0.15	0.050	0.001	0.003

Selected genes indicative of pigment cell identity or shared functions are shown.
doi:10.1371/journal.pone.0067801.t001

Table 2. Shared gene expression among melanocyte, RPE, and iridophore.

Gene	Melanocyte	RPE	Iridophore	Embryo	Notes
<i>rpl26</i>	22354.26	19692.74	23528.06	87.23	Ribosomal protein
<i>rps17</i>	12677.82	10420.73	16940.17	59.88	Diamond-Blackfan Anemia [90]
<i>rps2</i>	12516.82	9306.57	12379.31	89.39	Ribosomal protein
<i>rpl27a</i>	6506.97	5852.65	8537.27	48.50	Ribosomal protein
<i>slc45a2</i>	4415.88	2376.16	2801.48	0.20	<i>albino</i> locus [54,55]
<i>rps26l</i>	2338.29	2362.00	2596.78	23.08	Ribosomal protein
<i>ppp1r21</i>	263.06	227.24	202.38	1.77	Protein phosphatase
<i>crfb5</i>	237.93	329.44	301.82	1.19	Jak-STAT cytokine receptor
<i>LOC100535047</i>	217.00	212.13	135.05	0.40	Uncharacterized
<i>dhdh</i>	201.46	185.72	161.64	1.52	dihydrodiol dehydrogenase
<i>cyhr1</i>	150.55	157.36	138.95	0.87	cysteine/histidine-rich 1
<i>igf2bp2b</i>	133.81	97.93	128.56	0.75	mRNA-binding protein
<i>ghitm</i>	133.71	119.78	162.37	0.99	BAX inhibitor protein family
<i>her9</i>	126.24	85.17	120.90	0.71	NOTCH pathway
<i>fam168a</i>	89.26	78.21	73.66	0.44	Chemoresistance [91]
<i>comtb</i>	81.11	55.05	70.61	0.32	Dopamine degradation
<i>flkbp3</i>	75.26	59.48	79.66	0.01	Rapamycin binding protein
<i>mtbl</i>	65.94	36.58	48.31	0.32	Heavy metal resistance [92]
<i>pard3b</i>	53.47	62.57	46.53	0.38	Cell-cycle
<i>hbp1</i>	41.93	50.61	52.08	0.12	SOX-TCF-HMG family transcription factor
<i>zgc:158345</i>	31.67	43.92	59.38	0.31	Tyrosine phosphatase, PTEN C2 domain
<i>ccdc85al</i>	31.26	34.99	40.96	0.13	Uncharacterized, coiled-coil protein
<i>grma</i>	17.17	18.26	28.83	0.10	Glutamate receptor, GPCR
<i>mbd2</i>	16.57	16.03	16.31	0.13	Binds methylated DNA
<i>triobpl</i>	14.28	16.86	12.85	0.01	TRIOBP-like, actin organization [93]
<i>rnd2</i>	14.23	10.66	12.26	0.00	Rho GTPase, neurite branching [94]
<i>LOC100334991</i>	10.17	7.87	10.08	0.03	Uncharacterized
<i>zgc:136564</i>	5.94	9.00	5.30	0.04	C9orf64 homologue, unknown function

Shown are RPKM values for genes co-enriched among the three pigment cell types at a level 100-fold greater than whole embryos, within a 2-fold change of each other, with a minimum RPKM of 4.

doi:10.1371/journal.pone.0067801.t002

cell populations were screened through a 30 μ M cell filter (Partec, 04–0042–2316). Cells were analyzed and sorted with a Dako MoFlo cell sorter using a 120 μ M nozzle at a drop drive (DD) frequency of 22390 Hz. Cells were illuminated using a 488 nm laser. Cells were gated on two attributes to separate cells from each other and from cellular debris. Cellular debris was detected using forward and side scatter, selecting against the smallest particles (\sim 1 μ m or less). Cells were sorted based on detection using 510–530 nm and 575–595 nm filters, corresponding to FL1 and FL2 in Figure 1D, respectively. When excited by the 488 nm laser, the autofluorescence of iridophores is clearly detectable in these channels as a group of cells extending at a 45 degree line in the upper right quadrant. Melanocytes and RPE do not autofluoresce with this intensity when excited by the 488 nm laser, and cluster at the lower left of the FACS plot. Cells were collected into ice-cold DPBS with 2% FCS and kept on ice until mRNA extraction.

mRNA Extraction, cDNA Synthesis, and Illumina Library Preparation

Pigment cell cDNA library construction was as follows. For mRNA extraction the Dynabeads[®] mRNA DIRECT Kit (In-

vitrogen) was used per manufacturer's instructions. Following mRNA elution from the Dynabeads, first strand cDNA synthesis was performed using MMLV reverse transcriptase (Clontech) using an anchored polyT primer tailed with a universal primer sequence (See Table S3 for primer sequences and Figure 2 for pigment cell cDNA library construction overview.) A universal primer sequence was also added to the 3' end of the first strand by template switching, allowing for PCR-amplification of the resultant cDNA [43,44]. Following PCR amplification using the high fidelity polymerase LA Taq (TaKaRa, PCR cycle: 95C for 1 minute, followed by 20 cycles of 98C for 25 seconds, 60C for 1 minute, 68C for 20 minutes), cDNA was digested with AluI and RsaI restriction enzymes (NEB). Blunt-end enzymatic fragmentation of cDNA was used instead of sonication and gel extraction to minimize loss of sample material and eliminate the end-repair step of Illumina library preparation. Since this reduced representation strategy might miss short cDNAs that lack both restriction sites, we sought to avoid this by including enzyme recognition sites within the cDNA amplification primers. This allows for the inclusion of short cDNAs in our libraries. Standard Illumina library preparations followed, performed by the Genome Technology Access Center (GTAC) at Washington University in St. Louis ([PLOS ONE | www.plosone.org](http://</p>
</div>
<div data-bbox=)

Table 3. Shared gene expression among melanocyte and RPE.

Gene	Melanocyte	RPE	Iridophore	Embryo	Notes
<i>pmela</i>	15177.25	4244.20	148.90	0.57	<i>Silver mouse, fading vision zebrafish</i> [95]
<i>dct</i>	14134.12	6406.98	402.47	0.65	Melanin synthesis
<i>tyrp1b</i>	12354.09	3769.95	200.99	1.13	Melanin synthesis
<i>tyrp1</i>	2546.87	1474.07	71.46	0.03	Melanin synthesis
<i>rlbp1b</i>	1181.62	1212.86	48.19	0.26	Retinaldehyde binding protein
<i>mitfa</i>	1122.44	448.53	16.22	0.00	Melanocyte master regulator
<i>pah</i>	1081.84	485.25	35.79	23.60	Melanin synthesis
<i>stra6</i>	703.09	539.15	32.81	3.00	Retinol metabolism
<i>rgra</i>	300.56	504.34	27.16	0.21	GPCR
<i>msnb</i>	254.08	217.35	11.10	0.45	FERM family, RDX homologue
<i>fam213ab</i>	217.86	160.16	12.32	0.28	Antioxidant enzyme
<i>rbp1a</i>	148.55	137.02	8.74	1.79	Retinol binding protein
<i>slc24a4a</i>	141.08	89.64	7.63	1.26	Neural crest and RPE expression [96]
<i>zgc:114181</i>	122.41	128.26	6.71	0.58	Putative CNDP1 homologue
<i>mab21l2</i>	120.20	176.48	2.98	0.82	Eye development [97]
<i>LOC100004225</i>	105.78	52.37	3.46	1.32	Uncharacterized
<i>lratl</i>	105.09	96.40	3.52	0.39	Lecithin retinol acyltransferase
<i>oca2</i>	102.56	56.96	1.63	0.07	<i>Pinkeyed-dilution mouse</i> [98]
<i>kif21al</i>	96.64	104.62	4.16	0.82	Kinesin family member, <i>LOC100537698</i>
<i>dhrs11al</i>	95.71	130.88	6.86	8.45	Dehydrogenase/reductase SDR family
<i>cadm3</i>	87.46	116.23	4.88	0.12	Nectin family cell adhesion protein
<i>cdh2</i>	86.69	99.72	6.17	1.10	Cell adhesion
<i>slc24a5</i>	83.81	34.68	1.56	0.00	<i>golden locus</i> [99]
<i>s1pr1</i>	83.14	74.37	4.78	1.20	Rhodopsin family GPCR
<i>ctgf</i>	62.15	62.19	4.20	0.32	Secreted mitogen
<i>fads6</i>	49.52	84.55	2.76	0.08	Fatty acid biosynthesis
<i>foxp4</i>	39.96	84.03	1.78	0.25	Neuronal arborization maintenance [100]
<i>foxb1b</i>	39.71	64.02	2.38	0.10	Forkhead box transcription factor
<i>kif21al</i>	37.47	58.20	3.21	0.37	Kinesin family member
<i>abcg2d</i>	34.72	48.81	1.58	0.00	<i>white</i> family member [101]
<i>LOC100149324</i>	33.08	31.15	1.55	0.14	Uncharacterized phospholipase
<i>efcab4b</i>	30.89	38.65	1.71	0.00	Calcium sensing GTPase
<i>col11a1a</i>	27.39	27.11	1.22	0.75	Collagen alpha chain precursor
<i>rdh13</i>	24.30	31.04	0.81	0.00	Retinol dehydrogenase
<i>cam4l</i>	23.38	37.54	1.34	0.29	Cell adhesion molecule 4-like
<i>srcrb4l</i>	21.14	20.88	1.18	0.80	Scavenger receptor Cys-rich group B-like
<i>col4a5</i>	20.86	29.39	1.69	0.49	Type IV collagen
<i>dao.2</i>	20.27	22.39	1.23	1.39	D-amino-acid-oxidase

RPKM values for genes co-expressed in melanocyte and RPE at least 10-fold greater than iridophores and whole embryos, with a minimum of 10 RPKM. doi:10.1371/journal.pone.0067801.t003

gtac.wustl.edu). In brief, a single A was added to the 3' end of each strand, Y-adapters ligated, and library enrichment PCR performed, followed by gel extraction size-selection for fragments ranging from 200–400 base pairs in length. Illumina library construction of pooled 3dpf embryos was performed by GTAC from total RNA extracted with Trizol reagent as previously described [45]. No PCR amplification of whole embryo cDNA was performed prior to Illumina adapter ligation and library enrichment. Sequencing was performed on the GAIIIX and HiSeq 2000 Illumina platforms. Technical sequencing replicates of the

same libraries on separate lanes were essentially identical (Figure S3).

Sequence Analysis

We used Novoalign (www.novocraft.com), to assign resultant expression sequence tags to a customized non-redundant database of cDNA sequences consisting of 25,102 known and predicted genes (Table S4). Initial inspection of the NCBI zebrafish mRNA database of 28,286 zebrafish cDNAs (ftp://ftp.ncbi.nih.gov/refseq/D_zebra/mRNA/Prot/) via an all-by-all BLAST search

Table 4. Shared gene expression among melanocytes and iridophores.

Gene	Melanocyte	Iridophore	RPE	Embryo	Notes
<i>syngn2l</i>	86.584	50.745	5.728	1.471	Unclear function, transmembrane protein
<i>tuba8l3</i>	78.779	132.465	11.725	0.397	<i>puma</i> locus [102]
<i>pcdh10a</i>	59.639	54.800	5.143	0.423	Neural crest expression [64]
<i>crestin</i>	16.922	25.646	2.214	0.145	Expressed repetitive element [60]
<i>LOC559216</i>	14.652	27.212	1.350	0.689	Uncharacterized RhoGEF
<i>si:dkey-72l14.7</i>	11.657	40.247	1.004	0.000	Rhodopsin family GPCR
<i>cdk15</i>	8.492	6.475	0.291	0.112	Cyclin dependent kinase
<i>emp3l</i>	6.859	17.644	0.293	0.046	Tumor suppressor [103]
<i>lamb1b</i>	5.486	6.138	0.630	0.427	Laminin-type EGF-like domains
<i>zgc:158328</i>	4.355	8.553	0.776	0.004	Uncharacterized, EMI and vWBF domains
<i>opn5</i>	3.824	1.796	0.193	0.000	Rhodopsin family GPCR
<i>ppfia2</i>	3.521	3.859	0.443	0.037	Axon guidance [104]
<i>rab27bl</i>	3.263	13.331	0.278	0.118	Melanosome transport [105]
<i>mc1r</i>	2.182	3.958	0.076	0.000	GPCR for melanocyte stimulating hormone
<i>birc7</i>	1.818	2.960	0.233	0.000	Inhibitor of apoptosis protein [106]

RPKM values for genes expressed in melanocytes and iridophores at least 5-fold greater than RPE and whole embryos.
doi:10.1371/journal.pone.0067801.t004

revealed multiple nearly identical sequences for cDNAs that would confound the unambiguous assignment of sequence tags. In order to generate a non-redundant cDNA database we selected single representatives for each gene as follows. In instances where a cDNA in the database resulted in a BLAST hit of greater than 94% identity to more than 70% the length of another transcript, we excluded the smaller of the two cDNAs. The resultant non-redundant zebrafish cDNA database contained 25,102 unique gene records. We further analyzed our non-redundant database by mapping all cDNAs onto the UCSC zebrafish browser (ZV9). Manual examination of 6 Mbs arbitrarily chosen along chromosome 13 revealed 130 annotated genes (combined RefSeq and Ensembl gene tracks). Of these, our non-redundant database identified 126. The 4 genes not represented in our database included 3 5 S ribosomal RNA genes and ENSDARG00000086970, an annotated gene with a predicted ORF but no clear orthology to other species. Thus, this test shows that our method to generate a non-redundant cDNA library results in a database that identifies ~99% of annotated genes (excluding ribosomal RNA genes). Furthermore, manual examination of our non-redundant library mapped onto this 6 Mb of chromosomal sequence revealed 10 sequences that were not annotated as RefSeq or Ensembl genes. Comparison to repeat tracks on the UCSC browser revealed that most (8/10) of these unannotated matches identified ORFs from repetitive, or retrotransposon DNA. It is not clear how these sequences were initially included in the NCBI cDNA database.

In summary, our efforts have generated a non-redundant zebrafish cDNA database that identifies most (~99%) of annotated genes, and includes 7% (10/126) records of dubious utility, but would tend not to confound RNA-seq analysis such as reported here. Sequencing results for each cDNA library are summarized in Table S1. For each cDNA library, the number of tags aligned to each gene was normalized by the length of the gene and the total number of uniquely aligning reads for that library using custom Perl scripts (reads per kilobase of cDNA per million mapped reads - RPKM [45]). Statistical calculations were performed in R (www.r-project.org). All sequencing data used in

this study are publicly available at NCBI's GEO database under accession GSE46387 (<http://www.ncbi.nlm.nih.gov/geo/query/acc.cgi?acc=GSE46387>).

Quantitative RT-PCR

Primers used for expression analysis are listed in Table S3, designed with NCBI's Primer-BLAST to be separated by at least one intron (<http://www.ncbi.nlm.nih.gov/tools/primer-blast/>). Expression data was normalized relative to beta actin for each sample, using cDNA produced as described above, without PCR amplification. Q-PCR was performed in a Perkin-Elmer thermocycler with the following conditions: 95C 1 min, 98C 20 sec, 60C 1 min, repeated for 40 cycles.

Results and Discussion

Purification of Melanocytes, Iridophores, and RPE from Whole Embryos to Generate Cell-specific Gene Expression Data

At three days post fertilization (dpf), melanocytes, iridophores, and the RPE are readily visible in zebrafish. Melanocytes are extensively dendritic, and identifiable due to the presence of black melanin. Iridophores are round reflective cells, easily seen with a microscope using incident light. The RPE is present in the eyes as a hexagonally packed layer of melanized cells. However, the percentage of melanocytes, iridophores, and RPE compared to all other cells in the fish is less than 1%, making cell-specific gene expression analysis from the whole organism difficult. Aided by a previously reported method using density gradient centrifugation to isolate melanocytes from the caudal fins of Blackmoor goldfish [20], we developed a simple procedure to rapidly purify these pigmented cells from zebrafish embryos. This procedure relies on the inherent densities of the melanin-filled melanocytes and RPE, and the guanine-filled iridophores. In brief, cells are enzymatically dissociated from intact fish, enriched for pigment cells via density gradient centrifugation, and sorted by flow cytometry using the autofluorescent property of iridophores (Figure 1). The other pigment cells in zebrafish, the peridone-containing xanthophores,

Table 5. Iridophore enriched genes.

Gene	Iridophore	Melanocyte	RPE	Embryo	Notes
<i>ifi30l</i>	2138.17	6.55	27.16	1.23	Melanoma antigen processing [107]
<i>fhl3</i>	1003.29	4.64	20.97	1.12	Actin organization [108]
<i>slc23l</i>	592.05	10.64	9.70	1.19	Nucleobase transport [109]
<i>gpnmb</i>	423.58	1.02	5.28	1.70	Glycoprotein [70]
<i>LOC100538040</i>	396.38	1.52	9.30	1.85	Uncharacterized, likely GPI-linked glycoprotein
<i>LOC100334697</i>	330.19	1.06	4.78	0.09	Crystal protein-like
<i>tpd52l1</i>	252.61	5.69	7.75	1.02	Membrane trafficking [110]
<i>LOC100535932</i>	221.28	0.98	4.64	0.18	Uncharacterized
<i>pltp</i>	145.30	1.07	2.02	0.02	Lipoprotein metabolism [111]
<i>LOC795494</i>	127.94	0.43	2.17	0.11	Nucleotide metabolism domain
<i>LOC100330987</i>	99.01	0.56	1.80	0.01	Uncharacterized
<i>zgc:77375</i>	94.86	0.44	2.24	0.01	Haloacid dehalogenase
<i>slc25a38a</i>	94.77	1.10	1.63	0.46	Mitochondrial carrier protein
<i>LOC100534970</i>	81.87	0.65	2.48	0.18	Uncharacterized
<i>tmem179bl</i>	79.07	0.32	0.66	0.14	Transmembrane protein
<i>fkbp15</i>	32.47	0.55	0.51	0.31	Uncharacterized
<i>pcolcel</i>	30.46	0.31	0.22	0.00	Extracellular matrix protein
<i>si:ch211-38m6.6</i>	28.42	0.12	0.23	0.00	Major Facilitator Superfamily
<i>tagln3b</i>	24.88	0.13	0.74	0.06	Cytoskeleton-associated [112]
<i>alx4b</i>	24.81	0.10	0.24	0.08	Skull ossification [89]
<i>hsf5</i>	21.07	0.05	0.20	0.00	Transcription factor
<i>osbpl10</i>	18.67	0.26	0.55	0.08	Intracellular lipid receptor
<i>si:dkey-225f23.4</i>	14.27	0.14	0.13	0.00	Uncharacterized
<i>zgc:112054</i>	12.99	0.34	0.40	0.00	bZIP transcription factor
<i>slc52a3</i>	12.73	0.03	0.12	0.12	Riboflavin transporter
<i>cart1</i>	9.87	0.19	0.28	0.00	ALX1 homolog
<i>myadm</i>	7.81	0.14	0.23	0.00	Myeloid associated differentiation
<i>znf831</i>	7.04	0.09	0.10	0.06	Zinc-finger double domain
<i>si:ch211-14k19.8</i>	5.80	0.06	0.09	0.00	Uncharacterized
<i>nfasc1</i>	5.27	0.07	0.11	0.00	Fibronectin domain

RPKM values for genes expressed in iridophores at least 30-fold greater than melanocytes and RPE, and 100-fold greater than embryos.
doi:10.1371/journal.pone.0067801.t005

do not pass through the density gradient and are not isolated by this method. Following cell purification, mRNA is isolated and Illumina libraries are constructed from cDNA (Figure 2). We purified melanocytes, iridophores, and RPE as described above and performed mRNA sequencing for 11, 5, and 5 independently isolated samples, respectively. In order to confirm the quality of our cell specific libraries, we assembled a list of genes known to be expressed in melanocytes, iridophores, and RPE. When we compared expression of these genes in our cDNA libraries to this control list, we observed expression corresponding to each cell type (Table 1). Furthermore, we also found good correlation for fold changes determined by qPCR of independently prepared biological samples and those determined by our RNA-seq data, indicating our RNA-seq fold change calculations between pigment cell types are realistic values (Figure S4). For instance, *ltk*, known to be a marker of iridophores, is highly enriched in iridophores compared to melanocytes (red square with x in Figure S4) [27]. Similarly, we find *dat*, a known requirement for melanogenesis, to be highly enriched in melanocytes and RPE relative to iridophores. Interestingly, we also find *rpe65a*, well-known to be

expressed in RPE, to also be expressed by melanocytes. This is not entirely surprising, as RPE65 is known to be present in keratinocytes, melanocytes, and melanoma, in addition to the RPE [46,47]. Thus, using this method, cDNA from melanocytes, iridophores, and RPE can be generated concomitantly from thousands of whole zebrafish embryos in a single day. The development of a fast and robust method for purifying these pigment cells greatly simplifies the production of multiple biological replicates needed for informative analysis of high-throughput expression data.

Analysis of Gene Expression in Melanocytes, Iridophores, and Retinal Pigmented Epithelium

We first aimed to use our RNA-seq data to identify the total number of genes expressed in each of the pigment cell types. To eliminate low-level background expression, we applied a baseline expression threshold of 1 read per kilobase of transcript per million reads (1 RPKM). We chose this threshold based on the ability to detect expression of known pigmentation and neural crest genes. For example, we found *mc1r*, *kita*, and *foxd3* to have RPKM values

Table 6. Guanine synthesis-related gene expression enrichment in iridophores.

Gene	RPKM				P-Value	
	Iridophore	Melanocyte	RPE	Embryo	Irid vs. Mel	Irid vs. RPE
<i>slc2a15a (GLUT5)</i>	48.55	0.16	0.73	0.28	7.66E-03	7.89E-03
<i>pgm2</i>	34.00	0.54	0.73	1.24	4.64E-03	4.68E-03
<i>dera</i>	3.67	0.98	0.39	2.76	3.40E-04	1.55E-04
<i>pfkp</i>	12.25	0.63	1.28	2.42	1.31E-02	1.53E-02
<i>aldoca</i>	6.22	0.04	0.00	0.83	2.50E-03	2.45E-03
<i>gapdhs</i>	1605.92	191.73	163.31	9.03	1.92E-02	1.79E-02
<i>pgk1</i>	281.34	146.41	125.46	38.36	9.05E-03	7.22E-03
<i>pgam1a</i>	587.26	216.58	158.84	32.46	1.13E-03	4.02E-04
<i>eno3</i>	1503.93	215.46	307.89	100.27	4.30E-08	4.09E-05
<i>pkm2a</i>	371.83	115.96	97.94	24.94	4.52E-04	2.83E-04
<i>ldhba</i>	440.62	74.53	44.46	72.72	2.70E-04	2.85E-04
<i>phgdh*</i>	1538.41	371.96	175.60	8.25	4.21E-03	2.22E-03
<i>psat1</i>	160.85	7.03	11.92	7.62	4.68E-03	3.85E-03
<i>psph</i>	2602.05	146.30	102.78	1.36	1.53E-03	1.38E-03
<i>shmt2</i>	86.02	5.37	5.92	2.83	9.83E-03	9.50E-03
<i>mthfd1</i>	177.66	7.98	8.41	13.99	2.71E-02	2.72E-02
<i>fh</i>	562.28	150.18	109.27	8.65	2.53E-02	1.81E-02
<i>mdh1a*</i>	3948.05	388.29	432.95	27.33	2.55E-05	1.48E-05
<i>pck2</i>	1.44	0.10	0.01	6.09	1.05E-02	8.50E-03
<i>aclya</i>	106.57	42.29	39.30	8.19	2.49E-03	1.72E-03
<i>rpia</i>	11.66	2.49	2.24	6.52	4.70E-03	3.89E-03
<i>prpsap1*</i>	95.27	35.48	24.12	3.13	3.13E-03	1.88E-03
<i>ppat</i>	49.23	2.49	3.72	7.89	4.22E-03	4.26E-03
<i>gart</i>	167.66	6.41	4.29	3.46	6.01E-03	5.72E-03
<i>pfas</i>	34.59	0.53	0.56	4.53	1.52E-03	1.51E-03
<i>paics</i>	1465.37	57.12	55.35	11.68	3.63E-03	3.50E-03
<i>adsl</i>	805.77	46.06	36.43	12.45	2.69E-03	2.38E-03
<i>atic</i>	467.16	7.60	9.63	18.34	1.01E-02	1.02E-02
<i>impdh1b</i>	816.19	11.45	21.98	1.06	1.30E-03	1.21E-03
<i>gmps</i>	102.41	3.86	5.14	6.35	1.15E-03	1.02E-03
<i>prtfdc1*</i>	309.88	1.56	3.10	0.00	1.39E-03	1.39E-03
<i>hpert1l</i>	21.31	0.25	1.13	15.99	7.28E-04	6.03E-04
<i>adssl</i>	0.73	1.04	1.75	6.82	2.61E-01	1.08E-01
<i>ak1</i>	87.12	228.27	149.74	40.66	4.24E-03	1.75E-01

RPKM values for enzymes related to guanine synthesis in iridophores. Enzymes are grouped with their commonly associated pathways. Rate-limiting enzymes from each of the specific pathways are indicated with an asterisk. Notably, *adssl* is the first adenine-specific gene in purine synthesis, and is not upregulated in iridophores. doi:10.1371/journal.pone.0067801.t006

assessment of the similarity of gene expression between melanocytes, RPE, and iridophores, we applied Pearson's Product-Moment Correlation test to the datasets. Because correlation values can be artificially skewed by outlying data points [49], we calculated the average correlation from 24,102 overlapping windows of 1000 genes, sorted by increasing whole embryo expression (Figure S6). Using this metric, we found the melanin-producing melanocytes and RPE were the most highly correlated ($r = 0.90$). The neural crest-derived melanocytes and iridophores were modestly correlated ($r = 0.52$). RPE and iridophores were also modestly correlated ($r = 0.49$). We expected the correlation to be dramatically lower when comparing a single purified cell type to whole embryos than when comparing two purified pigment cell

types to each other. We thus determined the correlations of each pigment cell type to mRNA-seq data from whole 3dpf zebrafish. By this general assessment, melanocytes, RPE, and iridophores are distinct from whole embryos, with average correlation values less than 0.02. Presumably, this low value (0.02) reflects the baseline correlation component from expression of housekeeping genes shared by all cells, and greater values (0.4–0.9) reflect shared specific gene expression among the pigment cell types.

Gene Expression Indicative of a Pigment Cell Identity

These correlations described above suggest there are genes enriched in all three pigment cell types that are generally indicative of pigment cell identity. It is not clear *a priori* which

genes should be shared by different pigment cell types. In order to construct an informative set of genes for this purpose, we searched for those that are expressed within a 2-fold change of each other at a minimum of 4 RPKM, and at least 100-fold greater than whole 3dpf embryos. We found 28 genes fulfilled these criteria (Table 2). Remarkably, 4 of the top 5 highest expressed genes on this list are ribosomal proteins. Pigment cell enrichment of ribosomal components is not surprising, considering several mouse coat color mutants are ribosomal proteins, although they are not the ribosomal components enriched here [50–53]. We also find the zebrafish *albino* gene (*slc45a2*) to be among the highest expressed genes in each of these pigment cell types [54,55]. The expression of *slc45a2* in iridophores is interesting, considering *albino* fish are not reported to have an iridophore defect. One possibility is that SLC45A2 performs a common role for organelle pH homeostasis in pigment cells. However, *in situ* analysis reveals no enriched expression in xanthophores, suggesting that *slc45a2* expression is not shared by all pigment cells [55]. This list of co-expressed genes also contains several other unexpected members, including the Jak-STAT cytokine receptor *cfb5*, and the BAX-inhibitor protein *ghim*. It is not clear what roles these genes play in pigment cells, but this list provides a starting point for understanding their shared functions in pigment cell biology.

Gene Expression Indicative of Cellular Function or Developmental Origin

We were also interested to identify genes that were enriched in only two pigment cell types that would reveal shared function or developmental origin. For this analysis, we filtered for shared expression of genes in two cell types at least 2-fold over the third cell type, where differences exceeded a significance of $p < 0.05$. Upon validation of expression differences via qPCR between pigment cell genes and whole embryos, we found a systematic bias of overcalling the fold changes between pigment cell values and whole embryos (Figure S7). Based on this result, we also required an 8-fold greater than embryo expression threshold for co-enrichment and cell-specific genes, as discussed below. Using these criteria, we found 214 genes were enriched in both melanocytes and RPE but not iridophores (Table S6), and 62 genes enriched in melanocytes and iridophores but not RPE (Table S7). Given that the RPE and iridophores do not share a pigment-type production or developmental origin, we expected fewer genes to be co-enriched in these cells, but not expressed by neural-crest melanocytes. Only one gene, *alcama* (also *dn-grasp* or *neuroilin-a*), the target of the zn-5/8 monoclonal antibody [56,57] was enriched in both RPE and iridophores when compared to melanocytes and whole embryos (Table S8). This is consistent with the notion there are few specific functions shared only between iridophores and RPE. It is intriguing that *alcama* has been found to mediate endothelin 1 signaling in cartilage development [58]. Relatedly, endothelin receptor (*ednrb1*) signaling is required for iridophore development in zebrafish [5]. It will be interesting to know whether *alcama* mutations have functional consequences in the iridophore or the RPE. Therefore, we suggest these lists of co-expressed genes are likely enriched for common metabolic functions, in the case of melanocytes and RPE, or developmental origins, in the case of melanocytes and iridophores.

Melanocyte and RPE Co-Expression

Due to their shared function of producing melanin and melanosomes, we expected many genes to be shared between melanocytes and the RPE when compared to iridophores. We found 214 genes that fit our parameters for shared enrichment (Table S6). As expected, there are many genes present involved in

melanin synthesis and melanosome biogenesis, including *pmela*, *det*, *tyrp1b*, *tyrp1*, *pah*, and *slc24a5*. There are several transcription factors in this enrichment group, including three forkhead box (*foxo1b*, *foxp4*, and *foxg1b*) and five homeobox-containing transcription factors (*hmx1*, *hmx4*, *otx1a*, *otx2*, and *otx5*). Although not required for RPE development in zebrafish, *mitfa* is expressed in the RPE at a relatively high level, consistent with the reported ability of *mitfa* to promote pigmented fate in zebrafish retinas [59]. However, as we find most of the other transcription factors co-enriched in melanocytes and RPE are expressed at lower levels, it is interesting to speculate that one or more of these factors are able to compensate for *mitfa* specifically in the RPE. Thus, this co-enrichment set may identify a more comprehensive list of genes for melanocyte and RPE identity and melanosome biogenesis.

An additional finding apparent from the 38 most highly expressed genes co-enriched in melanocytes and RPE is that iridophores also express these genes, albeit at a much lower level (Table 3). The close developmental lineage relationship between melanocytes and iridophores suggests a possible “leakiness” of specificity that may result in weak expression of melanocyte genes in iridophores. This possibility is supported by the observation that the *parade* zebrafish mutant contains pigment cells with both melanocyte and iridophore characteristics [22].

Melanocyte and Iridophore Co-Expression

Because of the common developmental origin from the neural crest for melanocytes and iridophores, we speculated that neural crest-specific gene expression would be readily identifiable. We found 62 genes that were significantly upregulated in melanocytes and iridophores over RPE (Table S7). A list of the 15 genes expressed at least 5-fold greater than RPE and 10-fold greater than whole embryos is shown in Table 4. Included in this group are several well-known regulators and markers of neural crest and pigment cell development, including the transcription factors *sox10* and the expressed repetitive element *crestin* [60]. The well-known pigmentation gene *mc1r* is also expressed in iridophores and melanocytes. Also included is the cell adhesion molecule *pcdh10a*, which is expressed by migrating zebrafish neural crest cells, and acts as a tumor suppressor in several cancers [61–63]. We also find a retinoic acid nuclear receptor subfamily member (*rxrga*) previously reported to be expressed in neural crest tissues [64–67]. Because we find this known set of neural crest genes in this co-enrichment list, other unknown markers of neural crest identity are likely to be present. For instance, several transcription factors are in this enrichment set not previously reported in neural crest, including the forkhead box transcription factor *foxo1a*, as well as the cell cycle regulator *cdk15*. Thus, this list of genes co-enriched in melanocytes and iridophores may more broadly identify markers of neural crest origin.

Cell-Type Specific Gene Expression

We were also interested in determining gene expression specific to each cell type. Because melanocyte and RPE gene expression have been previously characterized, we do not discuss them in detail here, but present the data as the supplemental tables listed below [36–38,68,69]. For this analysis we required an expression level at least 2-fold over the other two cell types ($p < 0.05$), as well as 8-fold greater expression than whole embryos. This filtering strategy resulted in a list of 108 genes specifically enriched in melanocytes (Table S9) and 24 in the RPE (Table S11). To independently validate these enrichment sets, we generated separate biological samples for each cell type and compared expression of selected genes from the enrichment sets via qRT-PCR. We observed good correlation of RNA-seq and qRT-PCR

relative expression levels, indicating our RNA-seq data is a reliable indicator of the gene expression in these pigment cells ($r^2 = 0.75$, Figure S4). These data will be useful for further studies of melanocyte and RPE biology.

Iridophore Gene Enrichment

In contrast to melanocytes and RPE, the iridophore transcriptome has not previously been explored. Since iridophores produce a guanine-based pigment, rather than the melanin characteristic of melanocytes and RPE, we expected to find many genes to be specifically enriched in this cell type. This indeed turned out to be the case, with 346 genes passing our baseline threshold for enrichment (Table S10). Included in this enrichment list are several factors known to be important for iridophore development, including *ltk*, *ednrb1*, and *pmp4a* [5,26,27]. Also, in order to identify previously unreported genes that may play interesting roles in iridophores, we filtered our list to include genes expressed at least 30-fold greater than melanocytes and RPE, and 100-fold greater than whole embryos. Thirty genes met these criteria (Table 5). The third highest expressed gene on this list, *slc23l*, may act as a guanine transporter. In mammals, the SLC23 gene family has roles in transporting nucleobases, such as guanine, as well as vitamin C. It is not clear how this highly expressed iridophore gene identifies a unique role for vitamin C in the iridophore, but it is tempting to speculate a role in guanine transport, either to transport guanine into the cell, or perhaps to transport newly synthesized guanine into the reflecting platelet organelles. One surprise is the finding that *gpnmb* is highly enriched in the iridophore. Roles for GPNMB have been described for melanocytes, melanoma, and the pigmented iris in mammals, and it has been suggested to act both as a plasma membrane protein and a component of the melanosome [70]. Our finding that *gpnmb* is more highly expressed in the iridophore than the melanocyte raises the possibility of a similar function in iridophore reflecting platelet organelle biogenesis. Also in this iridophore-specific enrichment list are six uncharacterized genes. Their enrichment in iridophores may aid in identifying functions for these proteins. We speculate that many iridophore-enriched genes will be indicative of novel cell-specific biological functions.

Many of the genes previously known to be expressed by iridophores are components of the purine synthesis pathway, as iridophore pigment largely consists of stacks of guanine plates [30,71]. Accordingly, we found a dramatic enrichment of enzymes comprising the pathway of guanine metabolism, from extracellular glucose import and glycolysis, through *de novo* synthesis and purine salvage (Table 6). When comparing iridophores to melanocytes and RPE, we find 5 facilitated glucose transporters, 7/11 steps of glycolysis, and 9/9 enzymes for *de novo* purine synthesis to be enriched. Given that iridophore pigment consists largely of guanine, one might expect the guanine pathway to be specifically upregulated. Consistent with this model, we found the split in the purine synthesis pathway at IMP to favor guanine production rather than adenine. The first guanine-specific enzyme, *impdh1b*, is expressed at a level 71-fold greater than melanocytes. In contrast, the first adenine-specific enzyme, *adssl*, is not significantly different from melanocytes or RPE, at 0.7-fold the level of melanocytes. Upon inspection of the known pathway of guanine production, we observed synthesis of guanine from GMP likely results in the recycling of 5-Phosphoribosyl 1-Pyrophosphate (PRPP), the rate-limiting substrate in purine synthesis (KEGG Pathway: dre00230). The enzyme responsible for this final step of guanine synthesis, *prtfdcl*, is enriched 198-fold over melanocytes ($p < 0.01$). From our expression data, we suggest a model of guanine pigment production in iridophores that illustrates a cycle of guanine

synthesis utilizing PRPP as a recycled carrier molecule (Figure 3). In this cycle, specific enzymes from glycolysis, the pentose phosphate pathway, serine/glycine metabolism, and the citrate cycle, are upregulated to coordinate the extensive guanine synthesis required for the reflective iridophore pigment.

Another question in iridophore biology is how the membranous platelets containing the reflective guanine crystals are formed. Our data suggests a likely contribution from ADP Ribosylation Factors (ARFs) and Rab GTPases. ARFs are a large family of ras-related GTPases that regulate membrane trafficking and organelle structure (For review see [72]). We find two ARF-related genes to be significantly enriched in iridophores compared to melanocytes and RPE, *arf6* and *arfip1*. Interestingly, we also found two members of the ras-related oncogene family to be enriched in iridophores; *rab27b* and *rab38*. Rab GTPases regulate many aspects of membranous vesicle formation and traffic [73]. In humans, Rab27 mutations cause hypopigmentation associated with the immunodeficiency disorder Griselli syndrome type II [74]. In addition, the formation of COPI transport vesicles is known to be mediated by the interaction of GAPDH with RAB2 [75]. Phosphorylation of GAPDH occurs through the Src/PI3K/AKT pathway, often downstream of receptor tyrosine kinase activation [76]. We found a single receptor tyrosine kinase enriched in iridophores, *ltk*, which we have previously shown to be required for iridophore development [27]. It is thus interesting to speculate that combined roles exist for GAPDH in both producing reactive carbonyl species during glycolysis for guanine production, as well as in forming the organelles within which iridophore pigment is contained.

Iridophores are a relatively less-studied pigment cell than melanocytes and RPE, and aside from the requirements for *foxd3*, *ednrb1*, and *ltk*, not much is known regarding the transcriptional regulation of iridophore identity. One might expect a single master regulator of iridophore identity, analogous to *mitfa* in melanocytes, which is highly expressed, to be readily identifiable in our data. However, we did not identify a highly expressed single candidate for a master regulator of iridophore identity. Instead, we found many moderately expressed transcription factors with known mouse or human orthologues to be significantly enriched in iridophores. Of these, there are several candidates that stand out as possible regulators of iridophore identity. One member of the basic helix-loop-helix (bHLH) family of transcription factors is specifically enriched in iridophores, *tfec*. Known to be expressed in iridophores, TFEC forms hetero and homodimers with other bHLH members and can function as a transcriptional activator or repressor [77–79]. Interestingly, there is one other bHLH in enriched in iridophores when compared to melanocytes and RPE, but it did not meet the 8-fold requirement over whole embryos. This gene, *myc11a*, is a paralog of the classic oncogenic protein MYC. A key component of iridophore identity is the upregulation of glycolysis and guanine synthesis enzymes. It is established that MYC upregulates glycolysis, DNA-synthesis, and nucleotide metabolism [80–82]. Another oncogene shown to regulate glycolysis and associated feeder pathways is Ets-1 [83]. The v-ets-erythroblastosis virus E26 oncogene homolog 1a (*ets1a*) is also highly enriched in iridophores. In mouse, *tfec* transcription is activated through multiple ets-binding domains in its promoter region, suggesting a conserved regulatory mechanism for ETS1A in *tfec* transcriptional regulation as well [84]. Further work will be necessary to determine whether TFEC and MYC11A coordinate the upregulation of guanine synthesis enzymes in iridophores.

We also find five homeobox-containing transcription factors are enriched in iridophores: *gbx2*, *cart1*, *alx3*, *alx4a*, and *alx4b*. Known to have several roles in the embryo and an early specifier of

posterior neural crest in *Xenopus*, gastrulation brain homeobox 2 (*gbx2*), is highly enriched in iridophores [85]. Remarkably, the other four homeobox transcription factors we identified are all aristaless-related; *cart1*, *alx3*, *alx4a*, and *alx4b*. Members of the Cart1/Alx3/Alx4 family of homeodomain proteins are known to regulate formation of skeletal elements in organisms ranging from sea urchin to mammals [86,87]. In humans, mutation and haploinsufficiency of ALX4 are associated with skull ossification defects [88,89]. It is not clear how these aristaless-related transcription factors might regulate iridophore identity, but recognizing their expression here will aid in understanding their function. Together, these iridophore-enriched transcription factors likely play key roles in regulating iridophore identity.

Conclusion

To contribute to the understanding of pigment cell biology, we have developed a method for rapidly and reliably purifying melanocytes, iridophores, and retinal pigmented epithelium from zebrafish embryos, followed by global gene expression analysis by mRNA sequencing. This work represents the first concomitant comparison of three pigment cell types and whole zebrafish embryos, which uniquely allowed us to identify co-expressed genes indicative of shared function or developmental origin, as well as those that are specifically enriched in single cell types. We thus have identified many genes previously not reported to be enriched in these pigment cell types. In particular, we discovered a dramatic upregulation of specific enzymes from several metabolic pathways that coordinate guanine synthesis in iridophores, along with many membrane-trafficking components and transcription factors that are likely critical for iridophore identity. This characterization of global gene expression data from multiple purified zebrafish pigment cell types will provide a resource for further biological analysis of these cells.

Supporting Information

Figure S1 RPE Correlations. Shown in (A) are the RPKMs of RPE_5_143hpf_32, which was collected at 143hpf, compared to the average RPKMs of RPE libraries 1–4, which were collected at 77–86hpf, for the 9029 genes detected at an average of 1–5000 RPKM across all five RPE libraries. Shown in (B) are the RPKM values for all genes detected between 1 and 5000 RPKM by RPE samples held at 25°C and 32°C. Magenta circles represent the 24 genes described as RPE-enriched in our analysis compared to iridophores, melanocytes, and whole embryos ($r = 0.95$).
(TIF)

Figure S2 Melanocyte Time Point Correlations. Shown are scatterplots of RPKM values for all genes expressed between 1 and 5000 RPKM by melanocytes collected at different time points.
(TIF)

Figure S3 Technical Replicate Correlation. Shown are scatterplots of RPKM values obtained for the technical sequencing replicates of sample Mel_3_77hpf. Sequencing runs 351 and 433 were single end reads of 36 and 42 nucleotides, respectively. 399s61 and 399s62 represent the two ends of a paired end 101 sequencing run.
(TIF)

Figure S4 Quantitative RT-PCR and mRNA sequencing expression data are correlated. Examined genes are indicated by object shape, as in the legend on the lower right. Cell type comparisons are indicated by color in the legend on upper left. The purple line indicates the position of perfect correlation. RNA-seq fold changes are computed directly for each

cell type comparison [i.e. $\log_2(\text{melanocyte RPKM}/\text{iridophore RPKM})$]. QPCR fold changes are calculated by first normalizing expression relative to beta actin, followed by the log transformation.

(TIF)

Figure S5 Transcriptome Coverage. The number of genes identified (y-axis) per number of sequence reads (x-axis) obtained is plotted for each sample used in this analysis. Technical replicates are shown as individual lines, colored by library type as indicated on the lower right. For example, the three green lines represent the three technical sequencing replicates of the pooled 3dpf whole embryos cDNA library. The dashed vertical line is at one million reads.

(TIF)

Figure S6 Pearson correlations of RNA-seq expression data. Genes are ordered by increasing whole embryo expression (Y-axis). Each point represents the correlation value for the 1000 gene-window between the indicated cell-type comparison, beginning at that position. The most highly expressed genes in whole embryos are ribosomal proteins, which correspond to a slight peak in correlation values when compared to melanocytes (lower right). The average Pearson correlations across all windows for each comparison are indicated on the right, with corresponding horizontal lines.

(PDF)

Figure S7 Whole embryos RNA-seq fold change bias. QPCR-based fold change values demonstrate a systematic overcalling of fold change values upon comparison of randomly fragmented whole embryo cDNA libraries with reduced-representation pigment cell libraries. The purple line represents the position of perfect correlation.

(TIF)

Table S1 Sequencing Summary. Gross sequencing results for cDNA libraries used in this analysis, with their respective developmental time points at 28.5C. Unless indicated, fish used for each library were held at 25°C. The type of sequencing runs are indicated by the suffixes of technical replicate names: 351: single end 36, 433, 436, and 440: single end 42, 399s61 and 399s62: paired end 101. *Uniquely mapped to the Washington University non-redundant cDNA database. Tags that were not uniquely assigned to a gene typically mapped to polyA, genomic, and Illumina-adapter sequences. **Total RNA was used for Illumina library preparation of 20 pooled 3dpf embryos, resulting in a lower fraction of uniquely mapping sequences due to a large proportion of ribosomal RNA in library. Abbreviations: Mel - Melanocyte, Irid - Iridophore, RPE - Retinal Pigmented Epithelium, hpf - hours post fertilization, dpf - days post fertilization.

(XLSX)

Table S2 All Libraries RPKM. Normalized expression values (RPKM) for each of the libraries used in this analysis.

(XLS)

Table S3 Primers. Primers used for library preparation and qPCR analysis.

(XLSX)

Table S4 Non-redundant cDNA database. Sequences for the genes used in this analysis.

(XLSX)

Table S5 Pigment Cell Expression AvgRPKM pValues. Averaged RPKM expression values for melanocyte, RPE, iridophore, and whole embryo. Also shown are Student's T-test

p-values, ensembl transcript and gene reference numbers, and the corresponding *zv9* genomic location of each gene.
(XLSX)

Table S6 Melanocyte & RPE Shared. Genes expressed by both melanocytes and RPE with an RPKM 2-fold greater than iridophores, and 8-fold greater than whole embryos.
(XLSX)

Table S7 Melanocyte & Iridophore Shared. Genes expressed by both melanocytes and iridophores with an RPKM 2-fold greater than RPE, and 8-fold greater than whole embryos.
(XLSX)

Table S8 RPE & Iridophore Shared. A single gene is expressed by both RPE and iridophores with an RPKM 2-fold greater than melanocytes, and 8-fold greater than whole embryos
(XLSX)

Table S9 Melanocyte Enriched Genes. Genes expressed in melanocytes 2-fold greater than RPE and iridophores, and 8-fold greater than whole embryos.
(XLSX)

References

- Henion PD, Weston JA (1997) Timing and pattern of cell fate restrictions in the neural crest lineage. *Development* (Cambridge, England) 124: 4351–9.
- Jin EJ, Erickson CA, Takada S, Burrus LW (2001) Wnt and BMP Signaling Govern Lineage Segregation of Melanocytes in the Avian Embryo. *Developmental Biology* 233: 22–37.
- Rawls JF, Johnson SL (2003) Temporal and molecular separation of the kit receptor tyrosine kinase's roles in zebrafish melanocyte migration and survival. *Developmental Biology* 262: 152–161.
- Lee H, Levorse JM, Shin MK (2003) The endothelin receptor-B is required for the migration of neural crest-derived melanocyte and enteric neuron precursors. *Developmental Biology* 259: 162–175.
- Parichy DM, Mellgren EM, Rawls JF, Lopes SS, Kelsh RN, et al. (2000) Mutational analysis of endothelin receptor b1 (*rose*) during neural crest and pigment pattern development in the zebrafish *Danio rerio*. *Developmental Biology* 227: 294–306.
- Carreira S, Goodall J, Aksan I, Rocca SA, Galibert M, et al. (2005) *Mitf* cooperates with *Rb1* and activates *p21Cip1* expression to regulate cell cycle progression. *Nature* 433: 764–9.
- Lang MR, Patterson LB, Gordon TN, Johnson SL, Parichy DM (2009) *Basonuclin-2* Requirements for Zebrafish Adult Pigment Pattern Development and Female Fertility. *PLoS Genetics* 5: e1000744.
- Rawls JF, Johnson SL (2001) Requirements for the *kit* receptor tyrosine kinase during regeneration of zebrafish fin melanocytes. *Development* (Cambridge, England) 128: 1–7.
- Botchkareva NV, Khlgatian M, Longley BJ, Botchkarev VA, Gilchrist BA (2001) SCF/c-kit signaling is required for cyclic regeneration of the hair pigmentation unit. *FASEB Journal* 15: 645–58.
- Nishimura EK, Granter SR, Fisher DE (2005) Mechanisms of Hair Graying: Incomplete Melanocyte Stem Cell Maintenance in the Niche. *Science* 307: 720–724.
- McNiven MA, Wang M, Porter KR (1984) Microtubule polarity and the direction of pigment transport reverse simultaneously in surgically severed melanophore arms. *Cell* 37: 753–65.
- Sheets L, Ransom DG, Mellgren EM, Johnson SL, Schnapp BJ (2007) Zebrafish melanophilin facilitates melanosome dispersion by regulating dynein. *Current Biology* 17: 1721–34.
- Laskin JD, Piccinini L, Engelhardt DL, Weinstein IB (1982) Control of melanin synthesis and secretion by B16/C3 melanoma cells. *Journal of Cellular Physiology* 113: 481–6.
- Patton EE, Widlund HR, Kutok JL, Kopani KR, Amatruda JF, et al. (2005) BRAF mutations are sufficient to promote nevi formation and cooperate with *p53* in the genesis of melanoma. *Current Biology* 15: 249–254.
- Saldana-Caboverde A, Kos L (2010) Roles of endothelin signaling in melanocyte development and melanoma. *Pigment Cell & Melanoma Research* 23: 160–70.
- Herrling T, Jung K, Fuchs J (2008) The role of melanin as protector against free radicals in skin and its role as free radical indicator in hair. *Spectrochimica Acta Part A: Molecular and Biomolecular Spectroscopy* 69: 1429–1435.
- Levin MD, Lu MM, Petrenko NB, Hawkins BJ, Gupta TH, et al. (2009) Melanocyte-like cells in the heart and pulmonary veins contribute to atrial arrhythmia triggers. *Journal of Clinical Investigation* 119: 3420–36.
- Plonka PM, Passeron T, Brenner M, Tobin DJ, Shibahara S, et al. (2009) What are melanocytes doing all day long...? *Experimental Dermatology* 18: 799–819.
- Linos E, Swetter SM, Cockburn MG, Colditz GA, Clarke CA (2009) Increasing Burden of Melanoma in the United States. *Journal of Investigative Dermatology* 129: 1666–1674.
- Clark CR, Taylor JD, Tchen TT (1987) Purification of Black Moor goldfish melanophores and responses to epinephrine. *In Vitro Cellular & Developmental Biology* 23: 417–21.
- Na GY, Pack SH, Park BC, Kim DW, Lee WJ, et al. (2006) Isolation and characterization of outer root sheath melanocytes of human hair follicles. *The British Journal of Dermatology* 155: 902–9.
- Kelsh RN, Brand M, Jiang YJ, Heisenberg CP, Lin S, et al. (1996) Zebrafish pigmentation mutations and the processes of neural crest development. *Development* (Cambridge, England) 123: 369–89.
- Mayer TC (1970) A comparison of pigment cell development in albino, steel, and dominant-spotting mutant mouse embryos. *Developmental Biology* 23: 297–309.
- Searle A (1968) Comparative genetics of coat colour in mammals. Logos Press Limited. 308 p.
- Ceol C, Houvras Y, Jane-Valbuena J, Bilodeau S (2011) The SETDB1 histone methyltransferase is recurrently amplified in and accelerates melanoma. *Nature* 471: 513–7.
- Curran K, Raible DW, Lister JA (2009) *Foxd3* controls melanophore specification in the zebrafish neural crest by regulation of *Mitf*. *Developmental Biology* 332: 408–417.
- Lopes SS, Yang X, Müller J, Carney TJ, McAdow AR, et al. (2008) Leukocyte Tyrosine Kinase Functions in Pigment Cell Development. *PLoS Genetics* 4: e1000026.
- Hitchings G, Falco E (1944) The Identification of Guanine in Extracts of *Girella nigricans*: The Specificity of Guanase. *Proc Natl Acad Sci USA* 30: 294–7.
- Rohrlich S, Rubin R (1975) Biochemical characterization of crystals from the dermal iridophores of a chameleon *Anolis carolinensis*. *The Journal of Cell Biology* 66: 635–45.
- Ng A, Uribe R, Yieh L, Nuckels R, Gross J (2009) Zebrafish mutations in *gart* and *paics* identify crucial roles for de novo purine synthesis in vertebrate pigmentation and ocular development. *Development* 136: 2601–11.
- Bharti K, Nguyen MT, Skuntz S, Bertuzzi S, Armheiter H (2006) The other pigment cell: specification and development of the pigmented epithelium of the vertebrate eye. *Pigment Cell Res* 19: 380–94.
- Strauss O (2005) The retinal pigment epithelium in visual function. *Physiological Reviews* 85: 845–81.
- Runkle EA, Antonetti DA (2011) The blood-retinal barrier: structure and functional significance. *Methods Mol Biol* 686: 133–48.

34. Dridi S, Hirano Y, Tarallo V, Kim Y, Fowler BJ, et al. (2012) ERK1/2 activation is a therapeutic target in age-related macular degeneration. *Proc Natl Acad Sci USA* 109: 13781–6.
35. Thompson DA, Gal A (2003) Genetic defects in vitamin A metabolism of the retinal pigment epithelium. *Developments in Ophthalmology* 37: 141–54.
36. Leung YF, Ma P, Dowling JE (2007) Gene expression profiling of zebrafish embryonic retinal pigment epithelium in vivo. *Investigative Ophthalmology & Visual Science* 48: 881–90.
37. Rizzolo IJ, Chen X, Weitzman M, Sun R, Zhang H (2007) Analysis of the RPE transcriptome reveals dynamic changes during the development of the outer blood-retinal barrier. *Mol Vis* 13: 1259–73.
38. Wistow G, Bernstein SL, Wyatt MK, Fariss R, Behal A, et al. (2002) Expressed sequence tag analysis of human RPE/choroid for the NEIBank Project: over 6000 non-redundant transcripts, novel genes and splice variants. *Mol Vis* 8: 205–20.
39. Grønskov K, Ek J, Brøndum-Nielsen K (2007) Oculocutaneous albinism. *Orphanet Journal of Rare Diseases* 2: 43.
40. Sprague J, Doerry E, Douglas S, Westerfield M (2001) The Zebrafish Information Network (ZFIN): a resource for genetic, genomic and developmental research. *Nucleic Acids Research* 29: 87–90.
41. Johnson SL, Nguyen AN, Lister JA (2011) *mitf* is required at multiple stages of melanocyte differentiation but not to establish the melanocyte stem cell. *Developmental Biology* 350: 405–13.
42. Kimmel CB, Ballard WW, Kimmel SR, Ullmann B, Schilling TF (1995) Stages of embryonic development of the zebrafish. *Developmental Dynamics* 203: 253–310.
43. Matz M, Shagin D, Bogdanova E, Britanova O, Lukyanov S, et al. (1999) Amplification of cDNA ends based on template-switching effect and step-out PCR. *Nucleic Acids Research* 27: 1558–60.
44. Zhu YY, Machleder EM, Chenchik A, Li R, Siebert PD (2001) Reverse transcriptase template switching: a SMART approach for full-length cDNA library construction. *BioTechniques* 30: 892–7.
45. Mortazavi A, Williams BA, McCue K, Schaeffer L, Wold B (2008) Mapping and quantifying mammalian transcriptomes by RNA-Seq. *Nature Methods* 5: 621–628.
46. Hinterhuber G, Cauza K, Brugger K, Dingelmaier-Hovorka R, Horvat R, et al. (2004) RPE65 of retinal pigment epithelium, a putative receptor molecule for plasma retinol-binding protein, is expressed in human keratinocytes. *J Invest Dermatol* 122(2): 406–13.
47. Amann PM, Luo C, Owen RW, Hofmann C, Freudenberger M, et al. (2012) Vitamin A metabolism in benign and malignant melanocytic skin cells: importance of lecithin/retinol acyltransferase and RPE65. *J Cell Physiol* 193(2): 718–28.
48. Collins JE, White S, Searle SM, Stemple DL (2012) Incorporating RNA-seq data into the zebrafish Ensembl genebuild. *Genome Research* 22: 2067–78.
49. Fujita A, Sato JR, Demasi MA, Sogayar MC, Ferreira CE, et al. (2009) Comparing Pearson, Spearman and Hoeffding's D measure for gene expression association analysis. *Journal of Bioinformatics and Computational Biology* 7: 663–84.
50. Oliver ER, Saunders TL, Tarlé SA, Glaser T (2004) Ribosomal protein L24 defect in belly spot and tail (Bst), a mouse Minute. *Development (Cambridge, England)* 131: 3907–20.
51. Drapchinskaja N, Gustavsson P, Andersson B, Pettersson M, Willig TN, et al. (1999) The gene encoding ribosomal protein S19 is mutated in Diamond-Blackfan anaemia. *Nature Genetics* 21: 169–75.
52. Skarnes WC, Rosen B, West AP, Koutsourakis M, Bushell W, et al. (2011) A conditional knockout resource for the genome-wide study of mouse gene function. *Nature* 474: 337–42.
53. Hrabe de Angelis MH, Flaswinkel H, Fuchs H, Rathkolb B, Soewarto D, et al. (2000) Genome-wide, large-scale production of mutant mice by ENU mutagenesis. *Nature Genetics* 25: 444–7.
54. Tsetschlhadze ZR, Canfield VA, Ang KC, Wentzel SM, Reid KP, et al. (2012) Functional assessment of human coding mutations affecting skin pigmentation using zebrafish. *PLoS ONE* 7: e47398.
55. Dooley CM, Schwarz H, Mueller K, Mongera A, Konantz M, et al. (2012) Slc45a2 and V-ATPase are regulators of melanosomal pH homeostasis in zebrafish, providing a mechanism for human pigment evolution and disease. *Pigment Cell & Melanoma Research* doi: 10.1111/pcmr.12053.
56. Fashena D, Westerfield M (1999) Secondary motoneuron axons localize DM-GRASP on their fasciculated segments. *J Comp Neurol* 406(3): 415–24.
57. Trevarrow B, Marks DL, Kimmel CB (1990) Organization of hindbrain segments in the zebrafish embryo. *Neuron* 4(5): 669–79.
58. Choudhry P, Joshi D, Funke B, Trede N (2011) Alcama mediates Edn1 signaling during zebrafish cartilage morphogenesis. *Developmental Biology* 349(2): 483–93.
59. Lane BM, Lister JA (2012) *Otx* but not *mitf* transcription factors are required for zebrafish retinal pigment epithelium development. *PLoS ONE* 7: e49357.
60. Rubinstein AL, Lee D, Luo R, Henion PD, Halpern ME (2000) Genes dependent on zebrafish cyclops function identified by AFLP differential gene expression screen. *Genesis* 26: 86–97.
61. Zhong X, Zhu Y, Mao J, Zhang J, Zheng S (2012) Frequent epigenetic silencing of PCDH10 by methylation in human colorectal cancer. *Journal of Cancer Research and Clinical Oncology* doi: 10.1007/s00432-012-1353-5.
62. Bertrand KC, Mack SC, Northcott PA, Garzia L, Dubuc A, et al. (2011) PCDH10 is a candidate tumour suppressor gene in medulloblastoma. *Child's Nervous Syst* 27: 1243–9.
63. Li Z, Li W, Xie J, Wang Y, Tang A, et al. (2011) Epigenetic inactivation of PCDH10 in human prostate cancer cell lines. *Cell Biology International* 35: 671–6.
64. Thisse C, Thisse B (2005) High Throughput Expression Analysis of ZF-Models Consortium Clones. ZFIN Direct Data Submission (<http://zfin.org>).
65. Tallafuss A, Hale LA, Yan Y, Dudley L, Eisen JS, et al. (2006) Characterization of retinoid-X receptor genes *rxra*, *rxra*, *rxrb* and *rxrg* during zebrafish development. *Gene Expression Patterns* 6: 556–65.
66. Waxman JS, Yelon D (2007) Comparison of the expression patterns of newly identified zebrafish retinoic acid and retinoid X receptors. *Developmental Dynamics* 236: 587–95.
67. He C, Wang C, Li B, Xie F, Chen Y, et al. (2009) Tissue-specific and embryonic expression of the retinoid X receptors in *Sebastiscus marmoratus*. *Comparative Biochemistry and Physiology. Part B, Biochemistry & Molecular Biology* 154: 221–8.
68. Flockhart R, Webster D, Qu K, Mascarenhas N, Kovalski J, et al. (2012) BRAFV600E remodels the melanocyte transcriptome and induces BANC1 to regulate melanoma cell migration. *Genome Research* 22: 1006–1014.
69. An J, Wan H, Zhou X, Hu D, Wang L, et al. (2011) A Comparative Transcriptomic Analysis of Uveal Melanoma and Normal Uveal Melanocyte. *PLoS ONE* 6: e16516.
70. Tomihari M, Hwang S, Chung J, Cruz PD, Ariizumi K (2009) *Gpnmb* is a melanosome-associated glycoprotein that contributes to melanocyte/keratinocyte adhesion in a RGD-dependent fashion. *Experimental Dermatology* 18: 586–95.
71. Curran K, Lister JA, Kunkel GR, Prendergast A, Parichy DM, et al. (2010) Interplay between *Foxd3* and *Mitf* regulates cell fate plasticity in the zebrafish neural crest. *Developmental Biology* 344: 107–118.
72. Donaldson JG, Honda A (2005) Localization and function of Arf family GTPases. *Biochemical Society Trans* 33: 639–42.
73. Grosshans BL, Ortiz D, Novick P (2006) Rabs and their effectors: achieving specificity in membrane traffic. *Proc Natl Acad Sci USA* 103: 11821–7.
74. Bahadoran P, Aberdam E, Mantoux F, Busca R, Bille K, et al. (2001) Rab27a: A key to melanosome transport in human melanocytes. *The Journal of Cell Biology* 152: 843–50.
75. Tisdale EJ, Kelly C, Artalejo CR (2004) Glyceraldehyde-3-phosphate dehydrogenase interacts with Rab2 and plays an essential role in endoplasmic reticulum to Golgi transport exclusive of its glycolytic activity. *Journal of Biological Chemistry* 279: 54046–52.
76. Huang Q, Lan F, Zheng Z, Xie F, Han J, et al. (2011) AKT2 suppresses GAPDH mediated-apoptosis in ovarian cancer cells via phosphorylating GAPDH at threonine 237 and decreasing its nuclear translocation. *Journal of Biological Chemistry* 286: 42211–20.
77. Lister JA, Lane BM, Nguyen A, Lunney K (2011) Embryonic expression of zebrafish *Mitf* family genes *tf3b*, *tf6b*, and *tfec*. *Developmental Dynamics* 240: 2529–38.
78. Chung MC, Kim HK, Kawamoto S (2001) TFEC can function as a transcriptional activator of the nonmuscle myosin II heavy chain-A gene in transfected cells. *Biochemistry* 40: 8887–97.
79. Mansky KC, Sulzbacher S, Purdom G, Nelsen L, Hume DA, et al. (2002) The microphthalmia transcription factor and the related helix-loop-helix zipper factors TFE-3 and TFE-C collaborate to activate the tartrate-resistant acid phosphatase. *Journal of Leukocyte Biology* 71: 304–10.
80. Yeung SJ, Pan J, Lee MH (2008) Roles of p53, MYC and HIF-1 in regulating glycolysis—the seventh hallmark of cancer. *Cellular and Molecular Life Sciences* 65: 3981–99.
81. Albajar M, Gómez-Casares M, Llorca J, Mauleon I, Vaque JP, et al. (2011) MYC in chronic myeloid leukemia: induction of aberrant DNA synthesis and association with poor response to imatinib. *Molecular Cancer Research* 9: 564–76.
82. Liu Y, Li F, Handler J, Huang C, Xiang Y, et al. (2008) Global regulation of nucleotide biosynthetic genes by c-Myc. *PLoS ONE* 3: e2722.
83. Verschoor ML, Wilson LA, Verschoor CP, Singh G (2010) Ets-1 regulates energy metabolism in cancer cells. *PLoS ONE* 5: e13565.
84. Rehli M, Lichanska A, Cassady AI, Ostrowski MC, Hume DA (1999) TFEC is a macrophage-restricted member of the microphthalmia-TFE subfamily of basic helix-loop-helix leucine zipper transcription factors. *The Journal of Immunology* 162: 1559–65.
85. Li B, Kuriyama S, Moreno M, Mayor R (2009) The posteriorizing gene *Gbx2* is a direct target of Wnt signalling and the earliest factor in neural crest induction. *Development* 136: 3267–78.
86. Etensohn CA, Illies MR, Oliveri P, De Jong DL (2003) *Alx1*, a member of the *Cart1/Alx3/Alx4* subfamily of Paired-class homeodomain proteins, is an essential component of the gene network controlling skeletogenic fate specification in the sea urchin embryo. *Development* 130: 2917–28.
87. Beverdam A, Brouwer A, Reijnen M, Korving J, Meijlink F (2001) Severe nasal clefting and abnormal embryonic apoptosis in *Alx3/Alx4* double mutant mice. *Development* 128: 3975–86.
88. Mavrogiannis LA, Antonopoulou I, Baxová A, Kutilek S, Kim CA, et al. (2001) Haploinsufficiency of the human homeobox gene *ALX4* causes skull ossification defects. *Nature Genetics* 27: 17–8.

89. Wuyts W, Cleiren E, Homfray T, Rasore-Quartino A, Vanhoenacker F, et al. (2000) The ALX4 homeobox gene is mutated in patients with ossification defects of the skull (foramina parietalia permagna, OMIM 168500). *Journal of Medical Genetics* 37: 916–20.
90. Cmejla R, Cmejlova J, Handrkova H, Petrak J, Pospisilova D (2007) Ribosomal protein S17 gene (RPS17) is mutated in Diamond-Blackfan anemia. *Human Mutation* 28: 1178–82.
91. Gu Y, Fan S, Liu B, Zheng G, Yu Y, et al. (2011) TCRP1 promotes radioresistance of oral squamous cell carcinoma cells via Akt signal pathway. *Molecular and Cellular Biochemistry* 357: 107–13.
92. Wu SM, Tsai PR, Yan CJ (2012) Maternal cadmium exposure induces mt2 and smtB mRNA expression in zebrafish (*Danio rerio*) females and their offspring. *Comparative Biochemistry and Physiology. Toxicology & Pharmacology* 156: 1–6.
93. Kitajiri S, Sakamoto T, Belyantseva IA, Goodyear RJ, Stepanyan R, et al. (2010) Actin-Bundling Protein TRIOBP Forms Resilient Rootlets of Hair Cell Stereocilia Essential for Hearing. *Cell* 141: 786–798.
94. Fujita H, Katoh H, Ishikawa Y, Mori K, Negishi M (2002) Rapostlin is a novel effector of Rnd2 GTPase inducing neurite branching. *The Journal of Biological Chemistry* 277: 45428–34.
95. Schonthaler HB, Lampert JM, von Lintig J, Schwarz H, Geisler R, et al. (2005) A mutation in the silver gene leads to defects in melanosome biogenesis and alterations in the visual system in the zebrafish mutant fading vision. *Developmental Biology* 284: 421–36.
96. Thisse B, Thisse C (2004) Fast Release Clones: A High Throughput Expression Analysis. ZFIN Direct Data Submission (<http://zfin.org>).
97. Kennedy BN, Stearns GW, Smyth VA, Ramamurthy V, van Eeden F, et al. (2004) Zebrafish rx3 and mab2112 are required during eye morphogenesis. *Developmental Biology* 270: 336–49.
98. Rinchik EM, Bultman SJ, Horsthemke B, Lee ST, Strunk KM, et al. (1993) A gene for the mouse pink-eyed dilution locus and for human type II oculocutaneous albinism. *Nature* 361: 72–6.
99. Lamason RL, Mohideen MA, Mest JR, Wong AC, Norton HL, et al. (2005) SLC24A5, a putative cation exchanger, affects pigmentation in zebrafish and humans. *Science* 310: 1782–6.
100. Tam WY, Leung CK, Tong KK, Kwan KM (2011) Foxp4 is essential in maintenance of Purkinje cell dendritic arborization in the mouse cerebellum. *Neuroscience* 172: 562–71.
101. Netter S, Fauvarque MO, del Corral RD, Dura JM, Coen D (1998) white+ transgene insertions presenting a dorsal/ventral pattern define a single cluster of homeobox genes that is silenced by the polycomb-group proteins in *Drosophila melanogaster*. *Genetics* 149: 257–75.
102. Larson TA, Gordon TN, Lau HE, Parichy DM (2010) Defective adult oligodendrocyte and Schwann cell development, pigment pattern, and craniofacial morphology in puma mutant zebrafish having an alpha tubulin mutation. *Developmental Biology* 346: 296–309.
103. Fumoto S, Hiyama K, Tanimoto K, Noguchi T, Hihara J, et al. (2009) EMP3 as a tumor suppressor gene for esophageal squamous cell carcinoma. *Cancer Letters* 274: 25–32.
104. Serra-Pagès C, Medley QG, Tang M, Hart A, Streuli M (1998) Liprins, a family of LAR transmembrane protein-tyrosine phosphatase-interacting proteins. *The Journal of Biological Chemistry* 273: 15611–20.
105. Chen Y, Samaraweera P, Sun T, Kreibich G, Orlow SJ (2002) Rab27b association with melanosomes: dominant negative mutants disrupt melanosomal movement. *The Journal of investigative dermatology* 118: 933–40.
106. Ma L, Huang Y, Song Z, Feng S, Tian X, et al. (2006) Livin promotes Smac/DIABLO degradation by ubiquitin-proteasome pathway. *Cell Death and Differentiation* 13: 2079–88.
107. Rausch MP, Irvine KR, Antony PA, Restifo NP, Cresswell P, et al. (2010) GILT accelerates autoimmunity to the melanoma antigen tyrosinase-related protein 1. *Journal of Immunology* 185: 2828–35.
108. Coghill ID, Brown S, Cottle DL, McGrath MJ, Robinson PA, et al. (2003) FHL3 is an actin-binding protein that regulates alpha-actinin-mediated actin bundling: FHL3 localizes to actin stress fibers and enhances cell spreading and stress fiber disassembly. *The Journal of Biological Chemistry* 278: 24139–52.
109. Yamamoto S, Inoue K, Murata T, Kamigaso S, Yasujima T, et al. (2010) Identification and functional characterization of the first nucleobase transporter in mammals: implication in the species difference in the intestinal absorption mechanism of nucleobases and their analogs between higher primates and other mammals. *The Journal of Biological Chemistry* 285: 6522–31.
110. Thomas DD, Martin CL, Weng N, Byrne JA, Groblewski GE (2010) Tumor protein D52 expression and Ca²⁺-dependent phosphorylation modulates lysosomal membrane protein trafficking to the plasma membrane. *American Journal of Physiology. Cell Physiology* 298: C725–39.
111. Scholler M, Wadsack C, Metso J, Manavalan AP, Sreckovic I, et al. (2012) Phospholipid transfer protein is differentially expressed in human arterial and venous placental endothelial cells and enhances cholesterol efflux to fetal HDL. *The Journal of Clinical Endocrinology and Metabolism* 97: 2466–74.
112. Depaz IM, Wilce PA (2006) The novel cytoskeleton-associated protein Neuronal protein 22: elevated expression in the developing rat brain. *Brain Research* 1081: 59–64.